Liquid Crystals
Publication details, including instructions for authors and subscription information:
http://www.informaworld.com/smpp/title~content=t713926090

Photoracemization broadening of selective reflection and polarization band of glassy chiral-nematic films

Shaw H. Chen; Richard J. Jin; Dimitris Katsis; John C. Mastrangelo; Semyon Papernov; Ansgar W. Schmid

Online publication date: 06 August 2010

To cite this Article Chen, Shaw H. , Jin, Richard J. , Katsis, Dimitris , Mastrangelo, John C. , Papernov, Semyon and Schmid, Ansgar W.(2000) 'Photoracemization broadening of selective reflection and polarization band of glassy chiral-nematic films', Liquid Crystals, 27: 2, 201 — 209
To link to this Article: DOI: 10.1080/026782900202985
URL: http://dx.doi.org/10.1080/026782900202985

LIQUID CRYSTALS, 2000, VOL. 27, NO. 2, 201–209

Photoracemization broadening of selective reflection and polarization band of glassy chiral-nematic films

SHAW H. CHEN†‡§¶*, RICHARD J. JIN†‡, DIMITRIS KATSIS†‡,
JOHN C. MASTRANGELO‡¶, SEMYON PAPERNOV§
and ANSGAR W. SCHMID§

†Materials Science Program, ‡Department of Chemical Engineering,
§Laboratory for Laser Energetics,
and ¶NSF Center for Photoinduced Charge Transfer,
Center for Optoelectronics and Imaging, University of Rochester,
240 East River Road, Rochester, New York 14623-1212, USA

(*Received 7 May 1999; accepted 26 August 1999*)

Glass-forming liquid crystals consisting of a cyclohexane central core with (*S*)-1-phenylethylamine and (4-cyanophenyl)naphthalene pendants were synthesized as hosts for racemizable (*R*)-dinaphtho[2,1-*d*:1′,2′-*f*][1,3]dioxepin, a chiral dopant. Chiral-nematic films 14, 22, and 35 μm thick were prepared for thermal and photoinduced racemization at temperatures from 95 to 130°C, i.e. in the mesomorphic temperature range, over a period of hours to days. Spatially modulated photoracemization was accomplished with an insignificant contribution from the thermal process at temperatures around 100°C over a period of up to 3 h. With an absorbance per unit thickness of 6.2 μm^{-1} at 334 nm, the photochemical process was essentially confined to the irradiated surface, thereby setting up counter-diffusion of the two enantiomers through the film, and hence the pitch gradient as visualized by atomic force microscopy. The significantly widened selective reflection band was interpreted with the Good–Karali theory extended for a gradient-pitch film. Furthermore, the bandwidth was found to increase with decreasing racemization temperature or with increasing film thickness, further validating the presence of a pitch gradient as a result of controlled photoracemization.

1. Introduction

A thermotropic liquid crystal presents one of the four mesophases: nematic, smectic, chiral-nematic (i.e. cholesteric), and columnar. Doped with a chiral guest, a nematic compound forms a chiral-nematic mesophase characterized by the helical pitch length, p, and the sense (i.e. right- or left-handed) of helical twisting. A chiral-nematic film is capable of selectively reflecting unpolarized incident light, resulting in equal intensities of a transmitted and a reflected component with opposite handedness. The handedness of the chiral-nematic film is defined by the polarization state of the reflected component [1]. Although handedness of a chiral-nematic system, be it low molar mass or polymeric in structure, can not be predicted *a priori*, it is known that the two enantiomers of a chiral guest induced opposite handedness in a given nematic host [2]. A chiral guest is further characterized by its helical twisting power, namely, a measure of its ability to accomplish helical twisting in a given nematic host. In a sense, the nematic mesophase represents a limiting case of a chiral-nematic mesophase at $p \to \infty$. Therefore, any modifications performed on the chiral guest that affect its absolute configuration or helical twisting power may lead to a change in the character of the chiral-nematic mesophase. This has prompted intensive efforts to induce a reversible conversion between the nematic and chiral-nematic mesophase at room temperature with an ultimate goal of developing devices for optical switching, data storage, and information display. Interconversion between the right- and left-handed chiral-nematic mesophase has been demonstrated with circularly polarized light [3] or with unpolarized light at two distinct wavelengths [4]. Moreover, interconversion between the chiral-nematic and nematic mesophase has been demonstrated via irradiation with a combination of unpolarized and circularly polarized light [5]. Another interesting idea takes advantage of two photochemically interconvertible molecular states, one with a finite and the other with a vanishing helical twisting power [6].

Of the chiral guests that have been investigated, (*R*)-dinaphtho[2,1-*d*:1′,2′-*f*][1,3]dioxepin, a bridged binaphthyl derivative, possesses a high enough helical twisting power to produce a chiral-nematic fluid film with selective reflection and circular polarization in the

*Author for correspondence; e-mail: shch@lle.rochester.edu

visible region [7, 8]. Furthermore, it has been shown to be susceptible to photoracemization, resulting in the conversion of a chiral-nematic mesophase to a nematic mesophase [9]. The combination of these two properties provides a route to tunable selective reflection from blue to green, red, and the infrared region via photoracemization to a varying extent. This idea has been demonstrated with a chiral-nematic fluid stabilized with a polymer network containing an open binaphthyl group [10]. The present study was motivated by the potential of spatially modulated photoracemization for generating a pitch gradient. An effort was made to minimize thermal racemization during photoracemization, since the negligible temperature gradient across thin films tens of microns thick tended to destroy the desired pitch gradient. The spectral region of selective reflection of a gradient-pitch film would be significantly broadened over a constant-pitch film, according to Hajdo and Eringen's theory [11]. Broer *et al.* [12] introduced a pitch gradient on the basis of counter-diffusion between a chiral and a nematic monomer via photopolymerization induced from one side of the film. Here we demonstrate the realization of pitch gradient using glass-forming liquid crystals [13], which not only play a central role in spatially modulating photoracemization above glass transition temperature (T_g) but also permit the resultant pitch gradient to be frozen in the solid state by quenching to below T_g. Glass-forming liquid crystals represent an emerging class of organic materials capable of preserving various modes of molecular order characteristic of liquid crystals in the solid state without encountering spontaneous crystallization [14]. The ability to produce glassy chiral-nematic films with a selective reflection and circular polarization band tunable to a desired spectral region will be beneficial to optical technologies.

2. Experimental

2.1. *Reagents and chemicals*

All chemicals, reagents, and solvents were used as received from the Aldrich Chemical Company or VWR Scientific, with the following exceptions. Tetrahydrofuran (99%) was dried by heating at reflux over sodium in the presence of benzophenone until blue, then distilled. Silica gel 60 (EM Science, 230–400 mesh) was used for liquid chromatography.

2.2. *Material synthesis and characterization*

2.2.1. *Glass-forming liquid crystals (GLCs): chiral-nematic (**I**) and nematic (**II**)*

Compounds **I** and **II** were synthesized following scheme 1 using previously reported chiral and nematic alcohols [15, 16]: (*S*)-1-phenylethyl-4-[4-(2-hydroxyethoxy)benzoyloxy]benzamide, A, and 2-(3-hydroxypropyl)-6-(4-cyanophenyl)naphthalene, B. In anhydrous

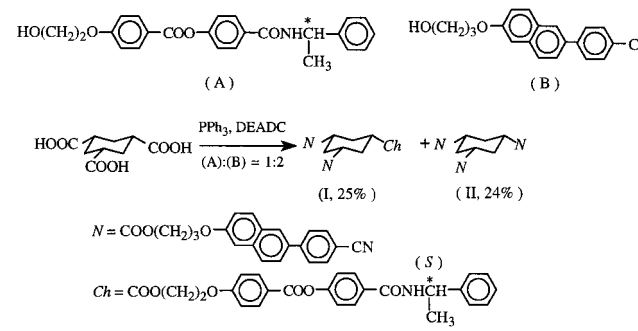

Scheme 1. Synthesis of chiral-nematic (**I**) and nematic (**II**) glass-forming liquid crystals.

tetrahydrofuran (28 ml) were dissolved A (1.21 g, 2.98 mmol), B (1.81 g, 5.95 mmol), *cis*-1,3,5-cyclohexanetricarboxylic acid (0.643 g, 2.97 mmol), and triphenylphosphine (PPh_3, 2.40 g, 9.12 mmol). Diethylazodicarboxylate (DEADC, 1.5 ml, 9.5 mmol) was then added dropwise, and the reaction mixture was stirred overnight. Solid residues collected upon evaporation of the solvent were dissolved in CH_2Cl_2 for column chromatography on silica gel, with a gradient elution from methylene chloride to 5 vol % acetone in methylene chloride. Repeated column chromatography under the same conditions, followed by precipitation from an acetone solution into methanol, afforded **I** in 0.866 g (25%) yield and **II** in 0.775 g (24%) yield. Other components could not be isolated from the statistical mixture of the reaction. NMR spectral data (in $CDCl_3$) for **I**: δ 8.30–6.95 (m, 32H, aromatic **H**), 6.40 (d, 1H, N**H**CH), 5.35 (m, 1H, NHC**H**CH_3), 4.50–4.10 (m, 12H, COOC$\mathbf{H}_2$ CH_2 C$\mathbf{H}_2$ O), 2.55–1.60 (m, 9H, cyclohexane ring), 2.20 (p, 4H, CH_2 C$\mathbf{H}_2$ CH_2), 1.65 (d, 3H, NHCHC$\mathbf{H}_3$). Anal. Calcd for $C_{73}H_{63}N_3O_{12}$: C, 74.67; H, 5.41; N, 3.58; found: C, 74.38; H, 5.58; N, 3.57%. NMR spectral data ($CDCl_3$) for **II**: δ 8.05–7.10 (m, 30H, aromatic **H**), 4.35 (t, 6H, COOC$\mathbf{H}_2$ CH_2), 4.15 (t, 6H, ArOC$\mathbf{H}_2$ CH_2), 2.50–1.55 (m, 9H, cyclohexane ring), 2.20 (p 6H, CH_2 C$\mathbf{H}_2$ CH_2). Anal. Calcd for $C_{69}H_{57}N_3O_9$: C, 77.29; H, 5.36; N, 3.92; found: C, 76.73; H, 5.40; N, 4.09%.

2.2.2. *(R)-Dinaphtho[2,1-d:1′,2′-f][1,3]dioxepin (**III**)*

Scheme 2 was followed for the synthesis of **III**. A reaction mixture containing (*R*)-1,1′-bi-2-naphthol (5.1 g, 17.5 mmol), dibromomethane (4.46 g, 25.7 mmol),

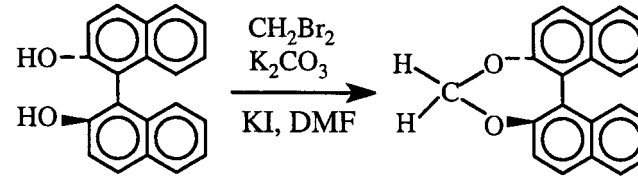

Scheme 2. Synthesis of (*R*)-dinaphtho[2,1-*d*:1′,2′-*f*][1,3]-dioxepin (**III**).

potassium carbonate (9.9 g, 71.6 mmol) and potassium iodide (0.33 g, 2.2 mmol) in 60 ml *N*,*N*-dimethylformamide was stirred at 60°C overnight. It was then shaken with diethyl ether (200 ml) and water (600 ml), and the organic layer was washed with 2% aqueous KOH (2×100 ml). After drying over anhydrous $MgSO_4$, the solvent was evaporated *in vacuo* before recrystallization from *n*-heptane to obtain **III** in 2.5 g (48%) yield, showing a crystalline melting point at 194°C, in comparison to 183–6°C reported previously [17]. NMR spectral data (in $CDCl_3$): δ 8.10–7.30 (m, 12H, aromatic **H**), 5.70 (s, 1H, acetal **H**). Anal. Calcd for $C_{21}H_{14}O_2$: C, 84.54; H, 4.73; found: C, 84.62; H, 4.87%.

2.2.3. *Chemical structures and thermotropic properties*

Chemical structures were elucidated with elemental analysis (performed by Oneida Research Services, Whitesboro, NY), FTIR (Nicolet 20 SXC) and H^1 NMR (QE-300, GE) spectroscopic techniques. Thermal properties were determined with a differential scanning calorimeter (Perkin-Elmer DSC-7) with a continuous N_2 purge at 20 ml min^{-1}. The reported transition temperatures were identified from second heating scans at 20°C min^{-1} of samples preheated to 250°C followed by quenching at -60°C min^{-1} to -30°C. The nematic and cholesteric mesophases were identified as threaded textures and oily streaks, respectively, under a polarizing optical microscope (Leitz Orthoplan-Pol) equipped with a hot stage (FP82, Mettler) and a central processor (FP80, Mettler).

2.3. *Glassy liquid crystalline films for racemization and optical characterization*

Binary and ternary mixtures of **I**, **II**, and **III** were prepared by codissolution in methylene chloride followed by filtration and thorough drying under vacuum, at room temperature overnight then at 150°C for 10 min. Fused silica substrates (1 in diameter $\times$ 1/8 in thick, Esco Products) transparent down to 200 nm were cleaned, spin-coated with Nylon 66, and uniaxially buffed using a polyaramide roller. Powdered samples were placed between two surface-treated substrates with the buffing directions parallel to each other. The film thickness was defined by glass fibre spacers (Bangs Laboratories). The actual thickness was verified to be within ± 0.5 µm of the nominal values with interference fringes of the air gap between the substrates gathered on a UV-Vis-NIR spectrophotometer (Perkin-Elmer Lambda 9). To maximize the mesomorphic order, all films were thermally annealed at 120°C for 30 min before quenching to room temperature. The thermal treatment did not lead to an appreciable extent of racemization (see the first paragraph in § 3). These pristine films were used for thermal and photoinduced racemization. Thermal racemization was conducted on a programmable hot plate at selected temperatures controlled to within ± 2°C. Photoracemization was performed at selected temperatures on the same hot plate plus a UV-lamp (B 100 AP, UVP, Inc.) equipped with a filter giving a sharp peak at 334 nm, where photoracemization was induced [9] and where the intensities were monitored. All experiments started with pristine films throughout the entire time periods. At the end of the experiments, the fluid films were quenched to room temperature for analysis.

For the interpretation of selective reflection by a chiral-nematic film, a nematic film 14 µm thick was prepared with compound **II** between a high (SF_6, $n_D = 1.805$) and a low (CaF_2, $n_D = 1.430$) index substrate, both treated as described above, and noting that a chiral-nematic film consists of a stack of helically twisted quasinematic layers. Following procedures reported elsewhere [18], the optical birefringence, $\Delta n = n_e - n_o$, and average index of refraction, $\bar{n} = (n_e + n_o)/2$, of the nematic film were determined as functions of wavelength. Note that n_e and n_o are the extraordinary and ordinary index of refraction, respectively. Values of Δn and $\bar{n}$ were then evaluated at specific wavelengths where the selective reflection bands were located. A thin film on the order of 100 nm was prepared on a fused silica substrate by spin-coating a 5 wt % toluene solution of a ternary mixture **I**:**II**:**III** = 1.00:4.36:0.55 at 2000 rpm followed by thorough drying. The film thickness measured on an interferometer (Zygo New View 100) together with the absorbance measured on the UV-Vis-NIR spectrophotometer yielded the absorption coefficient.

2.4. *Characterization of selective reflection and circular polarization*

A spectrophotometer was used to characterize selective reflection and circular polarization, both at normal incidence. Selective reflection spectra were collected using unpolarized incident light, and circular polarization spectra using right- and left-handed circularly polarized incident light generated by a combination of a linear polarizer (HPN'B, Polaroid) and an achromatic quarter waveplate (Meadowlark Optics). The light source of the instrument was found to be linearly polarized to some extent because of the grating system. To minimize potential artifacts, measurements were carried out with the buffing direction of the cell oriented vertically and horizontally. The arithmetic average of the two transmittances was reported as the selective reflection and circular polarization spectra [18]. Fresnel reflections from air–glass and glass–air interfaces were eliminated through the use of a reference cell comprising an index-matching fluid ($n_D = 1.500$ at 25°C, Cargille Laboratories) sandwiched between two surface-treated substrates.

2.5. *Imaging of cholesteric pitch by atomic force microscopy (AFM)*

A 22 μm film of a ternary mixture, **I**:**II**:**III** = 1.00:4.36:0.55, was prepared between a pair of fused silica substrates following the same procedure as described above, except the alignment coating was with poly(vinyl alcohol). The film was photoracemized at 140 μW cm^{-2} (334 nm) and 100°C for 2 h. Soaking in deionized water resulted in the separation of the substrates with most of the film staying on a single substrate. Immersing in liquid nitrogen produced flakes, which were mounted on a 1 cm steel disk with an adhesive for AFM imaging. The instrument (Nanoscope III, Digital Instruments, Inc.) comprises an extended multimode scanner capable of a lateral range of up to 80 μm and a silicon cantilever (Nanoprobe SPM, 308–315 kHz resonant frequency, Digital Instruments, Inc.) for tapping-mode operation. Selected areas of a flake's fracture cross section were mapped as both amplitude and phase scans. Raw data were processed using routines for contrast enhancement and low pass filtration to eliminate image clutter due to perturbations of the less than atomically smooth fracture surface and the piezo noise of the instrument.

3. Results and discussion

Compound **I** is a chiral-nematic GLC with T_g at 75°C and T_c at 88°C; compound **II** is a nematic GLC with T_g at 68°C and T_c at 195°C. For the investigation of thermal racemization, a mixture was prepared at a molar ratio of **II**:**III** = 1.00:0.15, showing T_g = 62°C and T_c = 169°C, although **III** is a crystalline solid with a melting point of 194°C. This mixture was used to prepare 14 μm thick films, yielding $\lambda_R = 710 \pm 10$ nm with a left-handed character. Thermal racemization was conducted on pristine films at 100, 110, 120 and 130°C. Because of the negligible temperature gradient across the thickness, thermal racemization was found to occur at a uniform rate, as suggested by the lack of band broadening. At the end of a given time period, t, the film was quenched to room temperature for the measurement of $\lambda_R(t)$. Over the range of $\lambda_R \geqslant 710$ nm encountered in the thermal experiment, direct proportionality was established between λ_R^{-1} and the mole fraction of **III** using a series of pristine samples. Therefore, it is legitimate to adopt λ_R^{-1} as a measure of the concentration of **III** in the analysis of racemization kinetics. The experimental data presented in figure 1 (*a*) reveal the first order kinetics, $\lambda_R(t)^{-1} = \lambda_R(0)^{-1} \exp(-2kt)$, where k is the rate constant characterizing the enantiomeric interconversion, $(R) \leftrightarrow (S)$. Note that the factor 2 in the exponential function above is intended to account for a loss of 2 moles of (*R*) for every mole converted to (*S*) as far as helical twisting is concerned. Based on the fitted k values from 100 to 130°C, the activation energy, E_{th} = 32.3 kcal mol^{-1}, was determined with the Arrhenius plot shown in figure 1 (*b*). This value is almost identical to that reported previously for a nematic liquid crystal host in the temperature range from 158 to 181°C [19]. The kinetic analysis also serves to assess the extent of thermal racemization accompanying photoracemization, which is the main thrust of this work.

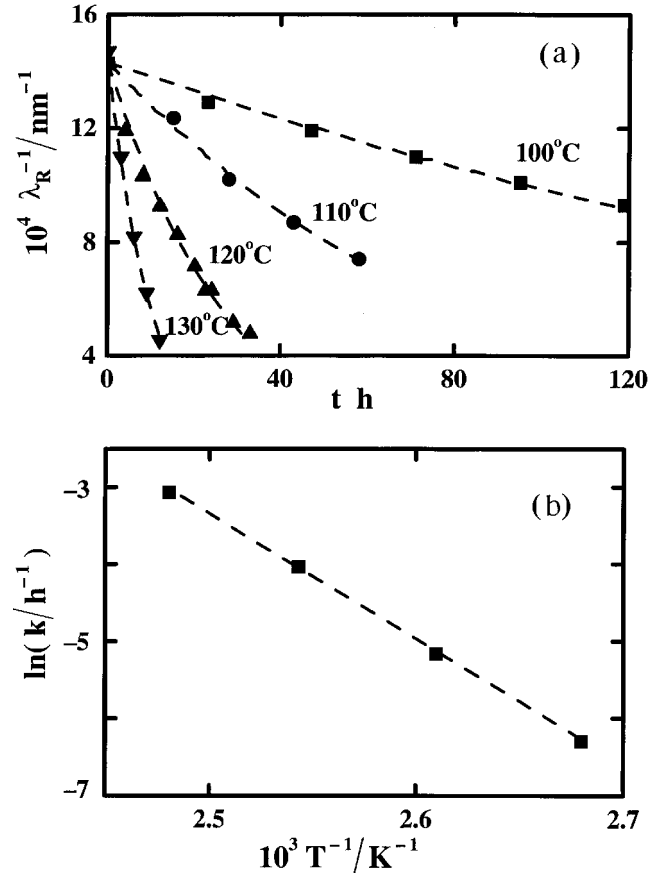

Figure 1. Films 14 μm thick of a binary mixture, **II**:**III** = 1.00:0.15, with T_g = 62°C and T_c = 169°C. (*a*) Thermal racemization kinetics as monitored by $\lambda_R(t)^{-1}$, serving to evaluate the kinetic constant $k(T)$ based on $\lambda_R(t)^{-1} = \lambda_R(0)^{-1} \exp(-2kt)$ represented as dashed curves; note that the experimental data are subject to a typical standard deviation of ± 5% of the mean. (*b*) The Arrhenius plot for the determination of the activation energy of thermal racemization of **III**.

A mixture at a molar ratio of **I**:**II** = 1.00:4.36 was used to prepare a 22 μm thick chiral-nematic film, giving λ_R = 1620 nm with a full width at half-height, $\Delta\lambda_R^o$ = 300 nm, identified as 'undoped' film in figure 2; note that superscript o signifies a pristine film. A ternary mixture was prepared at a molar ratio of **I**:**II**:**III** = 1.00:4.36:0.55, showing T_g = 65°C and T_c = 156°C. A 22 μm film of this mixture revealed pitch tightening, λ_R = 550 nm with $\Delta\lambda_R^o$ = 125 nm, shown as a solid curve in figure 2. Irradiation with a UV-source at 140 μW cm^{-2}

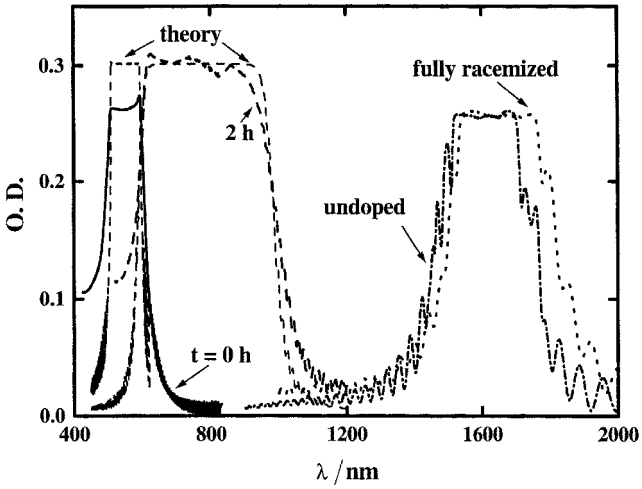

Figure 2. Selective reflection spectra of 22 μm films of a ternary mixture, **I**:**II**:**III** = 1.00:4.36:0.55, with T_g = 65°C and T_c = 156°C: solid curve, pristine film; dashed curve, photoracemized at 140 μW cm^{-2} (334 nm) and 100°C for 2 h; dotted curve, fully racemized film. The chain-dot curve is for a blank 22 μm film of a binary mixture, **I**:**II** = 1.00:4.36. Input data for the theoretical prediction: pristine film, $\bar{n}$ = 1.65, Δn = 0.26 and λ_R = 550 nm; partially racemized film, $\bar{n}$ = 1.62, Δn = 0.21, λ_R = 790 nm, and p (nm) = − 9.54x (μm) + 585, where x is the distance from the irradiated surface into the film.

(at 334 nm) of the doped film at 100°C for 2 h was found to untwist the pitch, yielding λ_R = 790 nm and $\Delta\lambda_R$ = 425 nm. According to figure 1 (*a*), it is evident that the extent of thermal racemization at 100°C over a period of 2 h is negligible in comparison with that of photoracemization. To drive the racemization process to completion, heating on a hot stage at 180°C was allowed for a period of 1 h. The selective reflection band of the 'fully racemized' film yielded λ_R = 1650 nm with $\Delta\lambda_R$ = 310 nm, nearly the same as that of the undoped film. The slight red-shift in λ_R from the undoped film can be attributed to dilution by the optically inactive guest upon complete racemization. In a recent publication, Brehmer *et al.* [20] has presented chiral-nematic polymers functionalized with menthone capable of the $E \rightarrow Z$ isomerization upon UV-irradiation. The geometric isomerization was accompanied by a significant loss of helical twisting power, leading to pitch loosening. Furthermore, the attendant band broadening was attributed to light scattering resulting from the loss of molecular orientation. Bobrovsky *et al.* [21] have made similar observations with a diminishing quality of selective reflection as pitch loosening and band broadening progressed with irradiation time. However, band broadening was attributed to photoisomerization occurring at the irradiated surface followed by macromolecular diffusion. It is noted that the chiral-nematic polymers used in both studies showed a T_g near ambient. Intrigued by the qualitative difference between the two sets of selective reflection spectra, figure 1 (*a*) of ref. [20] vs figure 9 of ref. [21], and by the fundamentally different interpretations, we placed our observation displayed in figure 2 in Hajdo and Eringen's perspective [11] by hypothesizing pitch gradient as the origin of band broadening.

The selective reflection spectrum of a pristine film (i.e. the solid curve in figure 2) was treated with Good and Karali's [22] theory constructed for a constant-pitch film. For light propagating through a constant-pitch film, $\lambda_R = \bar{n}p$ at normal incidence, where $\bar{n}$ is the average refractive index of quasi-nematic layers comprising the chiral-nematic film [23]. With Δn = 0.26 and $\bar{n}$ = 1.65 determined at 550 nm (see § 2), reasonably good agreement was secured between the theory and experiment as shown in figure 2. The fact that the observed optical density due to selective reflection falls short of the predicted value of 0.30 indicates a deviation from the perfect order in which all helical axes are oriented perpendicular to the substrate. The theory was then extended for the treatment of pitch gradient by numerically dividing the film into a large number of thin layers. Each layer was assigned a p value, and an infinitesimal step in p was allowed between neighbouring layers so that the entire film took on a prescribed pitch profile. The continuity of the electric and magnetic fields was ensured at the boundary between neighbouring layers. We opted for the Good–Karali approach over the Hajdo–Eringen formalism because of the ease of numerical implementation. It was found that dividing a 22 μm film into 100 layers is adequate to ensure numerical convergence of the computed spectrum. For the film irradiated at 100°C for 2 h, Δn = 0.21 and $\bar{n}$ = 1.62 were determined at λ_R = 790 nm (see § 2), and a pitch profile was implemented in the extended theory: p (nm) = − 9.54x (μm) + 585, where x denotes the distance from the exposed surface into the film. The pitch profile was established by imposing a linear relationship, as a first order approximation, between the bounding p values corresponding to the top edges of the observed selective reflection band. The predicted spectrum was found to agree very well with the experimental observation, as displayed in figure 2. In contrast, without the pitch gradient the bandwidth was underestimated by 84% in comparison with the experimental observation using the same values for Δn, $\bar{n}$, and λ_R. Thus, the selective reflection spectra have been successfully interpreted without resorting to adjustable parameters: pristine film with a constant pitch and partially photoracemized film with a gradient pitch.

The hypothesis of pitch gradient as the origin of band broadening was further tested by examining the effects of racemization temperature and film thickness. Photoracemization was conducted at 95, 100, and 105°C, all at 140 μW cm^{-2} for 2 h, to unravel the effect of

temperature. Note that while the rate of a photochemical process is inherently insensitive to temperature, molecular diffusivity generally decreases exponentially with decreasing temperature. The selective reflection spectra shown in figure 3 (*a*) indicate that the decreasing diffusivity of the guest is conducive to band broadening by limiting the extent of racemization (via counter-diffusion) towards the 'dark' side of the film. The same interpretation applies to the effect of film thickness: the bandwidth increases with increasing thickness, as shown in figure 3 (*b*). Note that the spectra for pristine films of all three thicknesses are nearly identical to each other; the spectrum from a 14 μm film is reproduced in figure 3 (*b*). The observed effects of temperature and thickness on bandwidth seem to be more consistent with the presence of a pitch gradient [11, 12] than light scattering [20]. Parts (*a*) and (*b*) of figure 3 combine to provide insight into the effect of irradiation intensity. Let us compare the spectra of two films, both 22 μm thick and subject to photoracemization at 105°C for 2 h with different irradiation intensities. Since these two films have slightly different chemical compositions, **I**:**II**:**III** = 1.00:4.36:0.55 vs 1.00:3.12:0.35, band broadening is characterized by $[(\Delta\lambda_R/\Delta\lambda_R^o) - 1] \times 100\%$, the % increase in bandwidth as a result of photoracemization. The bandwidth was found to increase by 90 and 160% at 33 and 140 μW cm^{-2} (at 334 nm), respectively. The rate of racemization at the exposed surface is expected to increase with increasing irradiation intensity, which will set up a steeper concentration profile of the (*R*)-enantiomer across the thickness at all times. For a wide band to emerge from controlled photoracemization, a steep concentration profile is desired. However, a steep concentration profile is expected to expedite the diffusion process. This is a problem involving diffusion with simultaneous chemical reaction, and the bandwidth can be optimized with respect to temperature, thickness and irradiation intensity for an intended application.

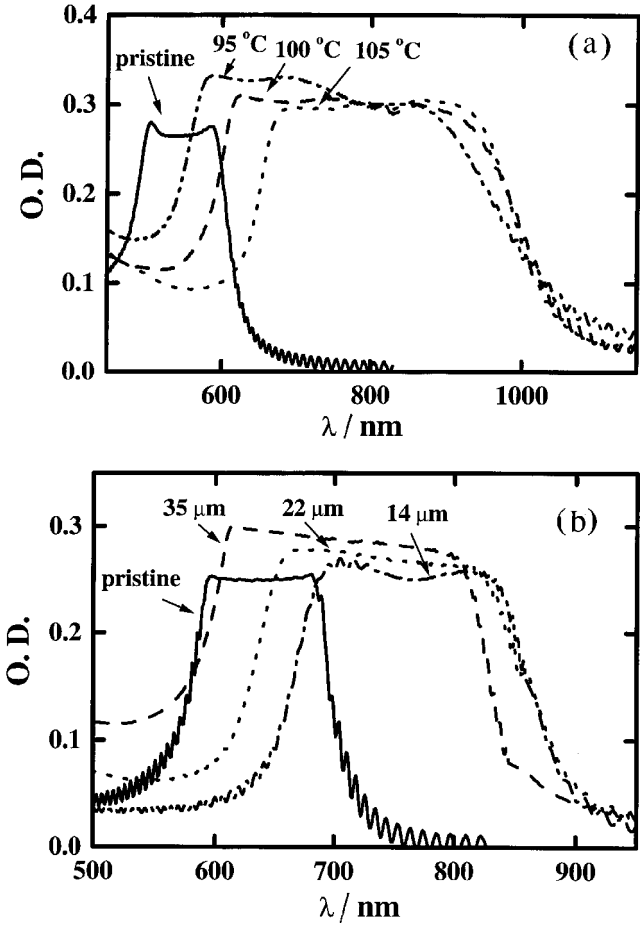

Figure 3. Selective reflection spectra. (*a*) Films 22 μm thick for **I**:**II**:**III** = 1.00:4.36:0.55 with T_g = 65°C and T_c = 156°C, photoracemized at 140 μW cm^{-2} (334 nm) for 2 h at 95, 100, and 105°C. (*b*) Films 14, 22, and 35 μm thick for **I**:**II**:**III** = 1.00:3.12:0.35 with T_g = 66°C and T_c = 156°C, all photoracemized at 33 μW cm^{-2} (334 nm) and 105°C for 2 h. The spectrum labelled as 'pristine' was taken from a 14 μm film.

To provide direct evidence of pitch gradient, a 22 μm film photoracemized at 140 μW cm^{-2} and 100°C for 2 h was freeze-fractured for characterization with atomic force microscopy (AFM). The AFM image of a 5.40 × 13.00 μm^2 section is shown in figure 4. With $p/2$ corresponding to the spacing between corrugations [24], p was estimated by taking an average over six corrugations. A value of 570 ± 20 nm was found towards the irradiated surface, which is in fairly good agreement with 585 nm located at the long wavelength edge of the selective reflection band shown in figure 2. Furthermore, the presence of a pitch gradient is evident from the AFM image; p was found to decrease from 570 to 420 nm over a depth of 13.00 μm into the film. Thus, the AFM technique is capable of semiquantitative analysis of the cholesteric pitch. However, our attempt to establish a pitch profile using the AFM image was hampered by the extent of scattering of the extracted values of p. To gain insight into how a pitch gradient originated from photoracemization, we probed the irradiation intensity profile in the film by measuring its absorbance per unit thickness, α, i.e. the absorbance per unit thickness. A 100 ± 10 nm film of the **I**:**II**:**III** = 1.00:4.36:0.55 mixture yielded $\alpha = 6.2\ \mu m^{-1}$ at 334 nm. Thus, the irradiation intensity diminishes by a factor of 1.6×10^6 after the first micrometer into the film. Consequently, racemization of the guest was photoinduced essentially at the irradiated surface, leaving the bulk of the film in the dark. The (*R*)-enantiomer near the irradiated surface was converted to the (*S*)-enantiomer as the photochemical process was initiated, thereby setting up a counter-diffusion of the two enantiomers across the film as stipulated by the

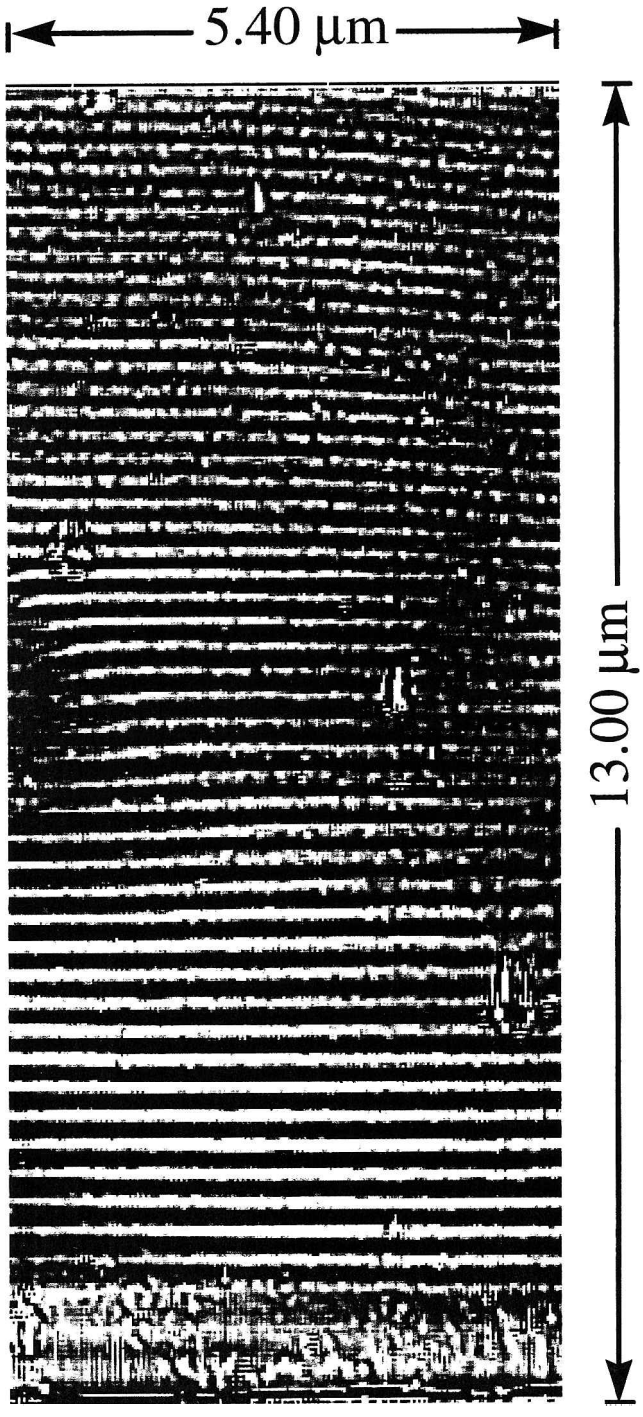

Figure 4. AFM image of a $5.40 \times 13.00\,\mu m^2$ section of a freeze-fractured flake from a 22 μm thick film of a ternary mixture, **I**:**II**:**III** = 1.00:4.36:0.55, upon photoracemization at $140\,\mu W\,cm^{-2}$ (334 nm) and 100°C for 2 h. Note that the bottom side of the flake was irradiated, giving rise to a longer pitch length than the top side.

conservation of mass. This process led to a pitch gradient across the film, with the 'dark' side of the film defining the short wavelength edge and the 'bright' side the long wavelength edge of the selective reflection band. The proposed mechanism may not support a linear pitch profile as implemented in the interpretation of bandwidth based on the extended Good–Karali theory. Nevertheless, the simplest profile accounting for a pitch gradient as the source of band broadening seems adequate for lack of a more sophisticated function.

It is well known that selective wavelength reflection of incident unpolarized light by a chiral-nematic film is accompanied by circular polarization [25]. The ability of a chiral-nematic film upon controlled photoracemization to produce broadband circular polarization is demonstrated in figure 5, which presents the transmittances of the right- and left-handed circularly polarized (RCP and LCP, respectively) incident beams. The degree of circular polarization is quantified with the dissymmetry factor, $g_e \equiv 2(I_L - I_R)/(I_L + I_R)$, in which I_R and I_L denote the right- and left-handed circularly polarized intensity, respectively. It is evident that $|g_e|$ equals 2 for perfect circular polarization. The spectrum shown for the film after 2 h photoracemization was used to calculate g_e, and a value ranging from -1.6 to -1.8 was obtained for the spectral region from 630 to 935 nm. Thus, a high degree of circular polarization over an extended spectral region has been accomplished. The quality of circular polarization and selective reflection after thermo- and photoracemization, as revealed in figures 2 and 5, indicate that the director of the quasi-nematic layers has remained parallel to the substrate. With (*S*)-1-phenylethylamine as the chiral building block of **I**, films prepared with a mixture of **I** and **II** present a left-handed structure, as indicated by the negative g_e values.

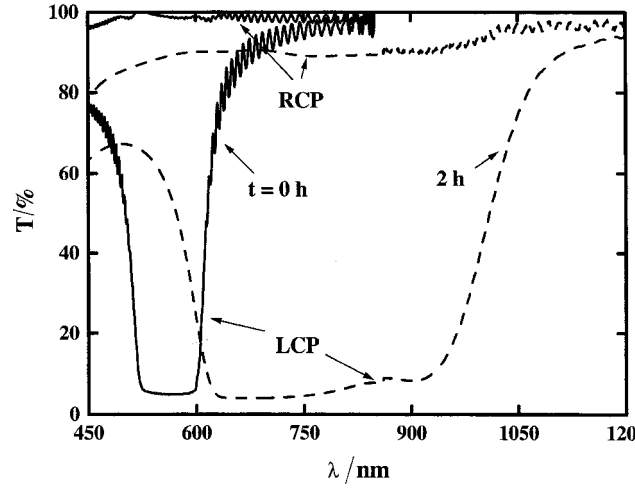

Figure 5. Circular polarization spectra measured with right- and left-handed circularly polarized (i.e. RCP and LCP) incident light on 22 μm films of a ternary mixture, **I**:**II**:**III** = 1.00:4.36:0.55, with T_g = 65°C and T_c = 156°C: solid curve, pristine film; dashed curve, photoracemized at $140\,\mu W\,cm^{-2}$ (at 334 nm) and 100°C for 2 h.

To assess the potential of the photochemically processed films for optical applications, exposure to UV-irradiation at 290 $\mu W\,cm^{-2}$ (at 334 nm) was allowed for days at room temperature (i.e. 40°C below T_g). That the selective reflection spectrum remained intact as a result of irradiation suggests the absence of racemization or the inability of the helical structure to respond to a decreasing concentration of the chiral dopant as racemization proceeds, an issue remaining to be resolved. In view of the absence of light absorption by **III** in the spectral region above 350 nm, exposure to visible or infrared is not expected to cause further racemization. In the present approach, counter-diffusion of the two enantiomers occurs in a chiral-nematic fluid of constant viscosity during photoracemization followed by thermal quenching to preserve the pitch gradient in a solid film. In contrast, the approach implemented by Broer *et al.* [12] involved counter-diffusion of two monomers, a nematic acrylate and a chiral diacrylate, in an increasingly viscous environment, in both time and space, as photopolymerization with crosslinking proceeds to freeze the pitch profile. Thus, the approach described here is more amenable to mathematical modelling and hence process optimization.

4. Conclusions

Glassy chiral-nematic films were prepared with (*S*)-1-phenylethylamine as an integral part of the molecular structure and with (*R*)-dinaphtho[2,1-*d*:1′,2′-*f*][1,3]-dioxepin as a racemizable dopant. These two chiral moieties were found to generate a left-handed helical structure in the nematic matrix consisting of (4-cyanophenyl)naphthalene. Racemization of the bridged binaphthyl dopant by thermal and photochemical means was conducted on films 14, 22, and 35 μm thick at temperatures from 95 to 130°C, i.e. 30 to 65°C above T_g, followed by quenching to room temperature to preserve the structure in the solid state. The effects of temperature, film thickness, and irradiation intensity on the bandwidth of selective reflection and circular polarization were investigated. The main observations are summarized as follows:

(1) The rate of thermal racemization of (*R*)-dinaphtho-[2,1-*d*:1′,2′-*f*][1,3]dioxepin followed first order kinetics with an activation energy of 32.3 kcal mol^{-1}. Photoracemization was found to predominate over thermal racemization at temperatures around 100°C.

(2) High degrees of circular polarization and selective reflection across a wide spectral region were accomplished via spatially modulated photoracemization. The broad selective reflection band was interpreted with the Good–Karali theory extended for a gradient-pitch film without recourse to adjustable parameters.

(3) The bandwidth was found to increase with decreasing temperature, increasing thickness, and increasing irradiation intensity. The effects of temperature and thickness on bandwidth further validated the hypothesis of pitch gradient as the origin of band broadening.

(4) With an absorbance per unit thickness of 6.2 μm^{-1} at 334 nm measured on a thin film, photoracemization was literally confined to the irradiated surface of the film. The concentration distribution of the (*R*)-enantiomer evolved with time via counter-diffusion across the film, resulting in a pitch gradient.

(5) The AFM image of the fractured film that had been photoracemized to a controlled extent revealed cholesteric pitch gradient. Moreover, the pitch length close to the irradiated surface estimated from the corrugations was found to be in fairly good agreement with that determined from the selective reflection band.

The authors wish to express their gratitude to S. D. Jacobs and K. L. Marshall of the Laboratory for Laser Energetics (LLE), University of Rochester, and T. J. Bunning of the Air Force Research Laboratory in Dayton, Ohio for their helpful discussion and technical assistance. The funding of this work was provided by the National Science Foundation under Grants CTS-9811172, CTS-9818234, and CHE-9120001. Additional support was provided by the Air Force Office of Scientific Research under Contract F49620-98-C-0060, the Department of Energy Office of Inertial Confinement Fusion under Cooperative Agreement No. DE-FC03-92SF19460 with LLE, and the New York State Energy Research and Development Authority. The support of DOE does not constitute an endorsement by DOE of the views expressed in this article.

References

[1] Born, M., and Wolf, E., 1980, *Principles of Optics*, 6th Edn (New York: Pergamon Press), pp. 28–30.
[2] Krishnamurthy, S., and Chen, S. H., 1992, *Macromolecules*, **25,** 4485.
[3] Huck, N. P. M., Jager, W. F., de Lange, B., and Feringa, B. L., 1996, *Science*, **273,** 1686.
[4] Feringa, B. L., Huck, N. P. M., and van Doren, H. A., 1995, *J. Am. chem. Soc.*, **117,** 9929.
[5] Suarez, M., and Schuster, G. B., 1995, *J. Am. chem. Soc.*, **117,** 6732.
[6] Denekamp, C., and Feringa, B. L., 1998, *Adv. Mater.*, **10,** 1080.
[7] Gottarelli, G., Hibert, M., Samori, B., Solladiè, G., Spada, G. P., and Zimmermann, R., 1983, *J. Am. chem. Soc.*, **105,** 7318.

[8] Ferrarini, A., Nordio, P. L., Shibaev, P. V., and Shibaev, V. P., 1998, *Liq. Cryst*., **24,** 219.
[9] Zhang, M., and Schuster, G. B., 1992, *J. phys. Chem*., **96,** 3063.
[10] Vicentini, F., Cho, J., and Chien, L.-C., 1998, *Liq. Cryst*., **24,** 483.
[11] Hajdo, L. E., and Eringen, A. C., 1979, *J. opt. Soc. Am*., **69,** 1017.
[12] Broer, D. J., Lub, J., and Mol, G. N., 1995, *Nature*, **378,** 467.
[13] Chen, S. H., Shi, H., Conger, B. M., Mastrangelo, J. C., and Tsutsui, T., 1996, *Adv. Mater*., **8,** 998.
[14] Chen, S. H., Katsis, D., Schmid, A. W., Mastrangelo, J. C., Tsutsui, T., and Blanton, T. N., 1999, *Nature*, **397,** 506.
[15] Shi, H., and Chen, S. H., 1994, *Liq. Cryst*., **17,** 413.
[16] Chen, S. H., Mastrangelo, J. C., Blanton, T. N., and Bashir-Hashemi, A., 1996, *Liq. Cryst*., **21,** 683.
[17] Deußen, H.-J., Shibaev, P. V., Vinokur, R., Bjørnholm, T., Schaumburg, K., Bechgaard, K., and Shibaev, V. P., 1996, *Liq. Cryst*., **21,** 327.
[18] Katsis, D., Chen, P. H. M., Mastrangelo, J. C., and Chen, S. H., 1999, *Chem. Mater*., **11,** 1590.
[19] Solladiè, G., and Zimmermann, R. G., 1984, *Angew. Chem. int. Ed. Engl*., **23,** 348.
[20] Brehmer, M., Lub, J., and van de Witte, P., 1998, *Adv. Mater*., **10,** 1438.
[21] Bobrovsky, A. Yu., Boiko, N. I., and Shibaev, V. P., 1998, *Liq. Cryst*., **25,** 393.
[22] Good, R. H. Jr., and Karali, A., 1994, *J. opt. Soc. Am. A*, **11,** 2145.
[23] De Vries, H., 1951, *Acta Crystallogr*., **4,** 219.
[24] Bunning, T. J., Vezie, D. L., Llyod, P. F., Haaland, P. D., Thomas, E. L., and Adams, W. W., 1994, *Liq. Cryst*., **16,** 769.
[25] Schadt, M., and Fünfschilling, J., 1990, *Jpn. J. appl. Phys*., **29,** 1974.